Journal of Power Sources 258 (2014) 195–203

Contents lists available at ScienceDirect

Journal of Power Sources

journal homepage: www.elsevier.com/locate/jpowsour

High throughput measurement of high temperature strength of ceramics in controlled atmosphere and its use on solid oxide fuel cell anode supports

Henrik Lund Frandsen*, Declan J. Curran, Steffen Rasmussen, Peter Vang Hendriksen

Department of Energy Conversion and Storage, Technical University of Denmark, Frederiksborgvej 399, DK-4000 Roskilde, Denmark

HIGHLIGHTS

- High temperature strength of functional ceramics was tested ×15 faster than state-of-the-art.
- Accurate assessment of strength statistics feasible with the high number of samples needed.
- High number of solid oxide fuel cell samples was tested at operating conditions.
- Accurate displacement and force measurements obtained by novel non-friction setup.
- Novel optical field methods used for accurate displacement assessment.

GRAPHICAL ABSTRACT

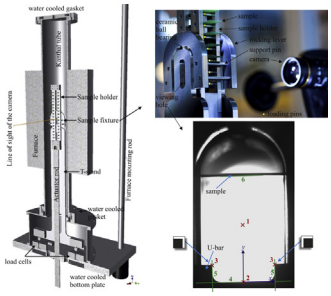

ARTICLE INFO

Article history:
Received 4 October 2013
Received in revised form
4 February 2014
Accepted 9 February 2014
Available online 18 February 2014

Keywords:
Strength
Ceramics
High temperature
Controlled atmosphere
Weibull statistics

ABSTRACT

In the development of structural and functional ceramics for high temperature electrochemical conversion devices such as solid oxide fuel cells, their mechanical properties must be tested at operational conditions, i.e. at high temperature and controlled atmospheres. Furthermore, characterization of the strength of ceramic components requires testing of a high number of samples due to stochastic failures. Successive heating and testing a single sample is very time consuming and consequently this hinders thorough studies with sufficient samples at operational conditions. This work presents a methodology for testing multiple samples at operational conditions providing a high throughput and thus the possibility achieve high reliability. Optical methods are used to measure deformations contactless, frictionless load measuring is achieved, and multiple samples are handled in one heat up. The methodology is validated at room temperature, and exemplified by measurement of the strength of solid oxide fuel cell anode supports at 800 °C.

1. Introduction

To allow fail-safe design of high temperature devices involving functional ceramics not only the electrochemical performance but also the strength distribution must be known. Hence, there is a need for effective methodologies for assessment of mechanical properties under conditions relevant for operation. Oxygen membranes, solid oxide fuel cells (SOFC) and solid oxide electrolysis cells are examples of such technologies, where knowledge of mechanical properties is crucial for their further development. In these fields new materials are developed and tested for their electrochemical properties. For application outside the lab, the integrity of the

* Corresponding author. Tel.: +45 4677 5668; fax: +45 4677 5858.
E-mail addresses: hlfr@dtu.dk, hlfrandsen@gmail.com (H.L. Frandsen).

http://dx.doi.org/10.1016/j.jpowsour.2014.02.036
0378-7753/

components is equally important, since mechanical failure of the components, in the mentioned applications, will have a severe influence on the performance, and often lead to global failure of the system. Hence, it is important for these technologies that relevant material and component data are available in the development and design process.

To analyze for failure, the strength is measured for a number of specimens, and strength distribution is characterized typically with a Weibull distribution [1–8]. Khalili and Kromp [9] concluded that measuring fewer than 30 samples leads to a large uncertainty and confidence interval of the parameters. Furthermore, for analyzing and designing against failure strength data are needed at a range of temperatures reflecting conditions during use. Thus, the number of measurements for a good statistical representation of the material/component becomes a challenge.

The typical approach for measuring the strength at high temperature is by mounting one sample at a time and going to high temperature where the sample strength is then probed [8,10–14]. This approach suffers from the drawback that the time needed to characterize each new material or component developed will be extensive. And only in Ref. [8] as much as the recommended 30 samples were measured at one temperature.

To minimize the time needed local heating concepts as e.g. by induction could be applied to reduce the time needed for each measurement, as typically only a small thermal mass needs to be heated. However, the mentioned technologies often have components that operate in an atmosphere different from air, which influences the composition and structure of the components. Thus, the atmosphere must be controlled to represent the operation conditions (see e.g. Ref. [2]), which complicates the local heating approach. Also too fast heating may induce micro cracks.

It is a fairly conventional task to control temperature and gasses in a controlled volume for experimentation, but it is challenging to measure force through a gas tight seal or gasket without encountering errors due to friction. The friction can be measured separately, but the friction might still be non-linear with applied load, and will therefore be different at the extra load in the actual testing. Thus, a better strategy is to avoid the use of gaskets or seals on the rods and transfer the load signal directly to the measurement device.

In this work a method which allows for; 1) testing of a high number of samples in one heat up, 2) testing in a controlled atmosphere, 3) measurement of the load in-situ to avoid friction, 4) optical measure of the displacements to avoid contact and error on force determination, is described and validated. The method is exemplified by measuring the strength of SOFC anode supports of Ni–3YSZ samples at room temperature and under operational conditions.

2. Experimental setup

The experimental setup is in house constructed and consists of (see Fig. 1):

- A gas tight Kanthal tube with two diametrically placed portholes for viewing into the furnace.
- A furnace around the center of the gas tight Kanthal tube.
- A cooling chamber where load cells are placed and which is directly connected with the gas tight tube.
- Two load cells (Model 41/000005, RDPE), which support the fixture to measure vertical loads.
- An external actuator (Model ET32, Parker) acting through a sealing ring in the bottom.
- A camera (Invenio-II 8D-C, Deltapix) with lens (LM50JC10M, Kowa) for displacement measurement by shooting through the portholes.

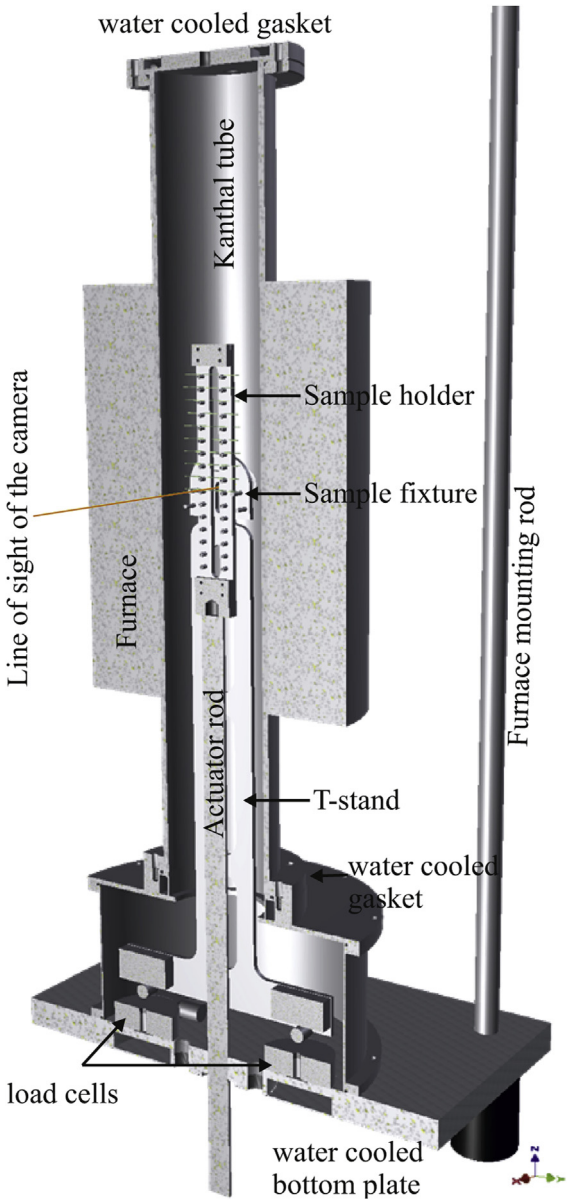

Fig. 1. 3D sketch of equipment showing the main components of the equipment.

- A fixture and combined sample holder for multiple samples manufactured in Inconel 600 (described further in Section 2.1).

2.1. Fixture for multiple samples

Various mechanical test methods are used to characterize the strength of ceramics; e.g. uniaxial tension and bending methods. The bending methods can both be axis symmetrical or non-axis-symmetrical.

The axis-symmetrical methods such as ball-on-ring and ring-on-ring results in multi-axial stress fields (see e.g. Refs. [15,16]), which must be accounted for in the analysis of the results. An advantage of these methods is that cutting flaws at the edge of the samples does not influence the strength measurement, as the stress is close to zero along the edge and much higher at the center of the sample. However, if it is the wish to investigate the actual strength of a technological component, which has cutting flaws, these methods are inadequate.

In the non-axis-symmetrical bending methods such as three point bending and four point bending, and in the uniaxial tension method, flaws at the edges will affect the strength measurement. This can in some cases as pointed out above be desired as to characterize "as prepared components", but if samples need to be cut to meet geometric requirements of the test method, the sensitivity to flaws along the cut is a drawback, as measured sample strengths may reflect more the cutting process than the material properties [17]. Thorough polishing of the samples along the cut can remove this effect. If the desire is to be able to test the influence of the cutting method at high temperature, the choice must be either bending methods or uniaxial testing.

Another difference between the bending methods and uniaxial tension method is that the so-called effective volume [18,19] is several times larger in the uniaxial tension method than those in the bending method of equally sized samples, as the entire volume is exposed to a uniform tension field.

As stated above, the aim here is to test more than 30 samples in order to obtain a good statistical representation of the material strength. In order to test the many samples within a reasonable time frame, multiple samples should be tested each time the furnace is brought to temperature. This is extremely challenging to achieve with uniaxial tension, and probably impossible at high temperature. Thus, as a compromise between the methods, the four point bending method is chosen for the ease of fixation.

Comparing results of this technique to others, proper scaling to account for size effects, i.e. different effective volumes must be done with the Weibull theory [16,18,20]. To achieve a large effective volume a large span is desired as well, but with the thin samples typically used for these applications (~300 μm [7]–1500 μm [21]) large deflections will occur. Hence, the sample size must be chosen in a compromise between maximizing the probed volume and minimizing complexities due to non-linear effects stemming from large deflections.

A special four point bending fixture was used for the purpose of testing multiple samples in one heat up. The center part of the fixture holds 16 samples for testing, and thus testing of 32 samples can be tested in two heating cycles. Fig. 2 shows an image of the fixture and how the samples are placed in a holder of 32 piece holder, each sample resting on two pings. These pins alternately serve as sample holders and as the two center loading pins in a four point bending, see Fig. 3.

Initially the holder with all the samples is placed above the two outer support pins. The actuator, on which the holder is mounted, moves the holder downwards until the two outer support pins lift the first sample. After further movement down, the two center pins above the present sample, starts to bend the sample in four point bending. Eventually the sample breaks and falls down, and the procedure is repeated until all samples are broken. Measurement of load and displacement for each sample is discussed below. The distance between the centers of the two inner pins is 25 mm and the distance between the centers of the two outer pins is 50 mm.

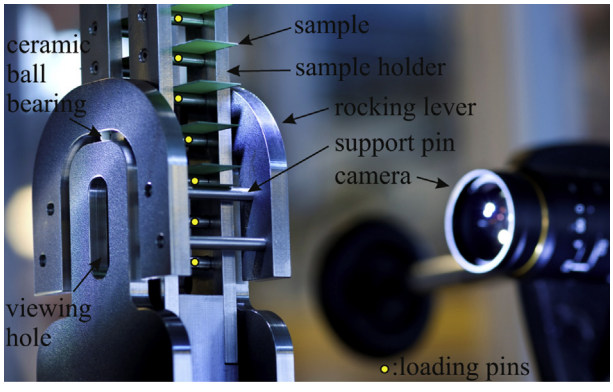

Fig. 2. Close up of fixture for multiple samples with camera in the background. The furnace is dismounted in this image.

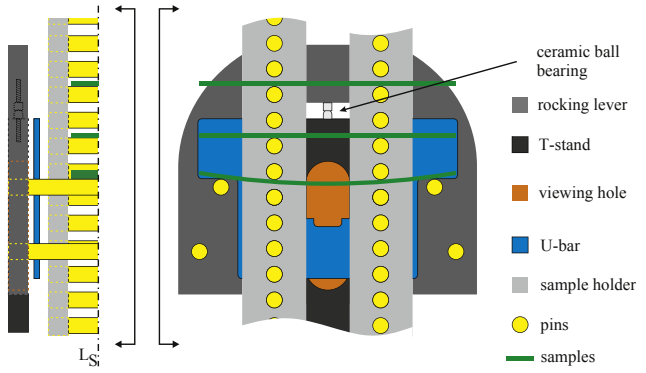

Fig. 3. Sketch of cross section through fixture with loaded sample and the fixture seen from the side. The arrows show the viewing angle taken to get from one viewpoint to the other.

2.2. Measurement of load

In the current setup the load cells are placed in a cooled chamber below the fixture. The cooled load cell chamber holds the same gas as the hot sample chamber. By placing the load cells inside the controlled atmosphere enclosure the difficulties of friction in the sealing around the loading rod is avoided. Heat is transferred between the sample chamber and the load cell chamber by conduction, radiation as well as by convection in the narrow slit between the heat shield and the T-shaped load transferring stand, see Fig. 4.

To ensure the temperature stays below the allowable maximum temperature of the load cells, water cooling is applied around the load cell chamber. Furthermore, the gas-inlet is located in the cold zone to force the convection upwards, see Fig. 4.

The load is generated by moving the actuator and the holder with the samples downwards. Doing so the inner pins move down, and the sample is put under an increasing stress as described in Section 2.1. This inner stress is balanced by an outer force to the actuator and an oppositely directed force through the T-shaped stand to the load cells. The load is transferred to the T-shaped stand through a horseshoe-shaped rocking lever, which ensures symmetric loading of the sample and provides visual access to the sample, see Fig. 3. The rocking lever rests on two ceramic pins, each of which consists of two zirconia screws. The heads of these screws have been machined to be dimple and cup shaped, thus functioning as a ball-bearings, see Fig. 3.

2.3. Measurement of displacements

The displacement can be estimated from the movement of the actuator, which has a digital gauge feeding back the displacement with an accuracy of approximately 0.1 μm. The actuator is however connected to the samples via a long rod made of Inconel 600 (as the remaining fixture). Moving this rod and the fixture in and out of the thermal field of the furnace, changes the thermal expansion of the rod. The thermal expansion depends on the thermal profile along the rod. However, assuming a constant thermal expansion coefficient, α, the extra movement of the sample due to changed length of the rod can be shown to be: where w is the actuator imposed

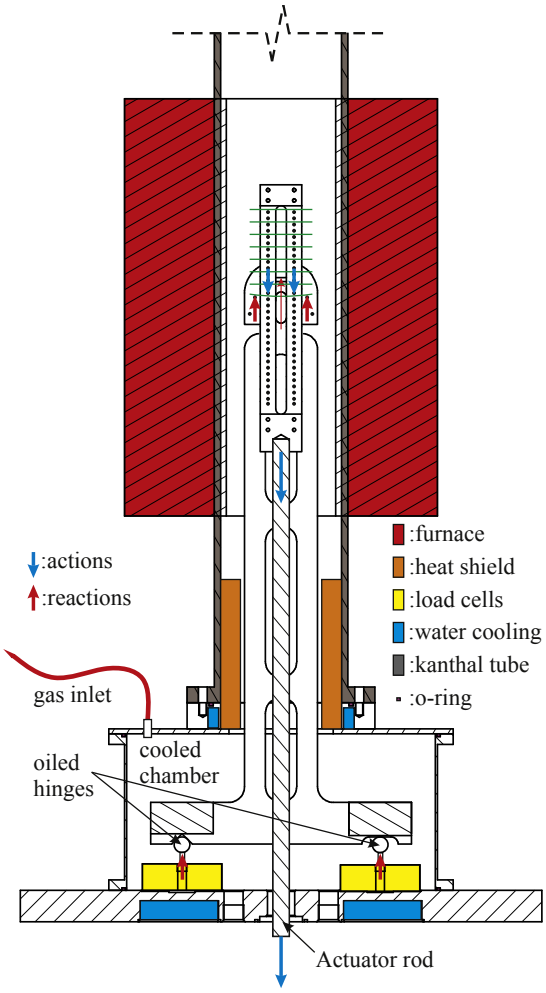

Fig. 4. Sketch of load transferring system, heat management system and atmosphere management.

movement, and ΔT is the total temperature difference from the bottom of the rod to the sample fixture.

This can be realized by considering that most of the rod remains in the same part of the thermal field, and it is only the bottom part of the rod, which experiences a new temperature. Figuratively speaking a movement of w could occur by cutting off a part (equal to the length of the movement) of the top of the rod and move it to the bottom of the rod. This part would thus experience the total thermal difference from top to bottom of the rod, ΔT. Hence the total displacement will be

$$w_{\text{total}} = w + w_{\text{T}} = (1 + \alpha \Delta T)w \quad (1)$$

The deviation between the total displacement and the measured actuator displacement is thus in the order of $800\ ^{\circ}\text{C} \cdot 14.6 \cdot 10^{-6}\ \text{K}^{-1} \approx 1\%$.

However, compliance of the fixture, ball-bearings, load cells etc. also constitute a possible source of error. This error could be estimated by using a very stiff sample. However, as described in the following, good accuracy can be reached by deducing the displacements from position measurements obtained by using a camera.

2.4. Optical detection of displacements

The displacements are measured by use of a camera, picturing the sample as it bends. The camera is located externally and has a line of vision through the portholes, which are located diametrically on each side of the central gas chamber tube, see Fig. 1.

The optical displacement measurement removes the above possible errors on the position measurements with a linear variable differential transformer (LVDT) and removes the error arising from compliance of the equipment. Especially when the LVDT is located external to the gas tight tube extra force must be applied to overcome the friction of a bellow or a sealing. External location also means that the probe rod, to which the LVDT is connected, must pass through a thermal field. Therefore, another reference probe is often applied to remove variations in thermal expansion of the equipment. Another good option for measuring displacement optically is by use of a line laser, which passes through the furnace, and detects the location of the sample. It should be noticed that none of the mentioned possibilities would be impossible to apply. The authors simply preferred the camera solution due to the additional possibility for visual inspection of the progress of the experiments.

In this work several techniques involving the different information in the image are applied in order to obtain as accurate a result as possible. These will be explained in the following.

2.4.1. Detection procedure

The overall strategy is to apply the known deformation shape in beam theory to the deformation of the beam in the image obtained from the camera. Thus the parabolic shape, which a beam under constant bending moment takes, is fitted to a series of points detected on the edge of the bending beam. Hereby the information at different points in the image is tied together, which improves accuracy relative to using the points individually. This of course relies on that the shape at large displacements does not deviate much from a second order parabola as the beam theory gives rise to.

To remove the error from thermal movements and small vibrations in the lab, a reference frame has been added to the images. The reference frame moves together with the supports of the sample, and the displacement of the sample is detected relative to this local frame rather than the global frame of the image itself. Physically the reference is a thin YSZ plate, which has been laser cut to the shape of a U-bar (referred to as U-bar in the following), see Fig. 3. The dimensions of the incision in the bottom of the U-bar is known and can be seen in the images, so it can be used for calibration and reference frame in all images.

To robustly detect the features in each image, and consequently accurately detect the edges for measuring, the following procedure is used (the different steps are illustrated in Fig. 5). First, the program approximately detects the:

1. Center of the backlit area by taking the average of the coordinates with high intensity.
2. Lower edge of the U-bar by locating a large intensity gradient below the center.
3. Corners of the incision in the U-bar by use of cross-correlation of sample images of the corners.

Knowing the approximate location of the features in the image is followed by accurate detection of the:

4. Edges at the sides of U-bar indent.
5. Edge at the bottom of the U-bar incision.
6. Specimen edge.

Finally, a local coordinate system ((x,y) in Fig. 5), which the displacements are related to, is located at the center of the U-bar bottom edge. At edge detection in 4, and 5, the fact that these edges

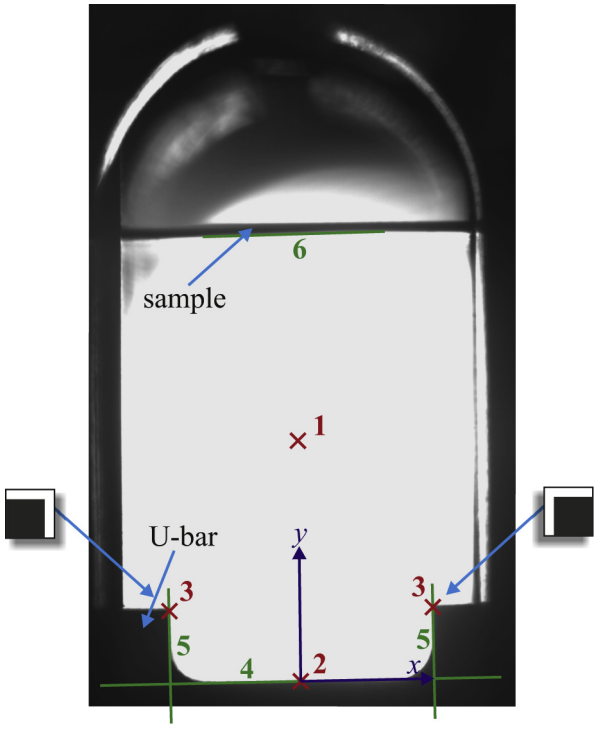

Fig. 5. Image from camera with identifiers for features and edges detection. The displacement detection procedure is explained in the text.

are perpendicular is exploited for higher accuracy of the fit as well. The edges are first found in pixel coordinates and consequently transformed to the local (x,y)-coordinate system. In this scaling the known distance between the two sides of the U-bar indent is used to scale the achieved distances in pixels to millimeters.

2.4.2. Edge detection

The edge detection of samples and fixtures is done by detecting points along the edge and by consequently fitting a line to the location of the points. A simple method to obtain the location of the edge would be to find the first pixel where the intensity deviated from the background intensity, I_b. However, this only allows for detection of the edge on pixel level, i.e. the location in whole numbers of pixels. To achieve sub-pixel resolution of the location the points are detected by fitting a piecewise function to the intensity variation across the edge. Good fits were obtained by the following function consisting of a constant part and a fourth order polynomial

$$I = \begin{cases} c_2(j-c_1)^4 + c_3(j-c_1)^2 + I_b \right) & \text{for} \quad j < c_1 \\ I_b & \text{for} \quad c_1 \geq j \end{cases} \tag{2}$$

where j is the pixel index along a line crossing the edge of interest, c_1, c_2 and c_3 are fitting parameters, and I_b is the background intensity. The location of the shift between the pieces of the function I, i.e. c_1, is also the location of the edge. In Fig. 6 an example of recorded pixel intensities across an edge with fits with Eq. (2) are shown.

2.4.3. Actuator displacement and optical detection

In Fig. 7 the optically detected maximum displacement of a solid oxide fuel cell specimen under different load levels are shown together with the maximum displacement estimated from the actuator displacement. The maximum displacement of the center of the beam, w_{max}, can be estimated from the actuator displacement, which is that at the loading points, w_{load}, by multiplying with the factor

$$\frac{w_{max}}{w_{load}} = \frac{\frac{Fa}{48EI}\left(3L^2 - 4a^2\right)}{\frac{Fa}{12EI}\left(3La - 4a^2\right)} = \frac{1}{4}\frac{3L^2 - 4a^2}{3La - 4a^2} \tag{3}$$

which equals 1.375 for the current setup with $a = L/4$.

Furthermore, in the calculation of the displacement shown in Fig. 7 the thermal expansion of the YSZ reference U-bar and the above discussed thermal contractions of the actuator rod moving out of the thermal field are accounted for.

The 0.7% higher displacement detected with the actuator, see Fig. 7, could be due to compliance of the equipment and load cells, or it could be a systematic error in the fitting method of the optical data explained in Section 2.4.2. Both explanations are possible,

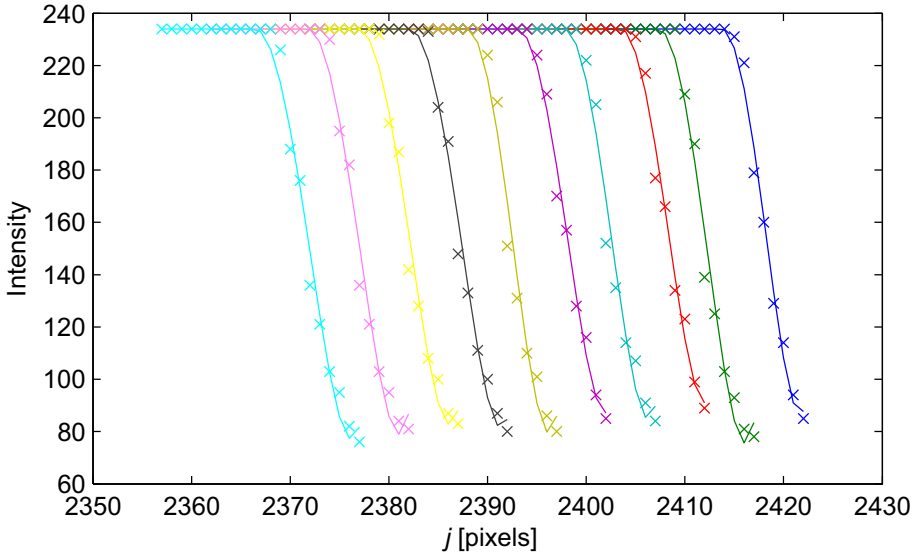

Fig. 6. Fitted intensity variations across a sample edge at several points along the edge. For clarity each intersection is plotted 5 pixels away from the former.

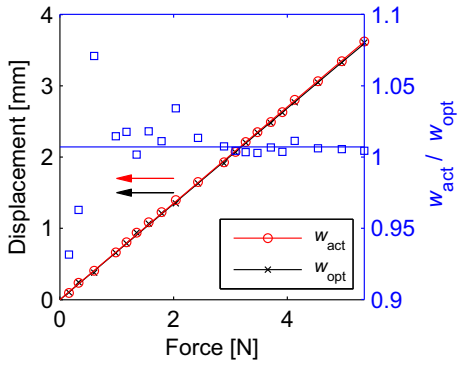

Fig. 7. Maximum displacement in different images shot at different loads, w_{opt}, together with the maximum displacement estimated from actuator movement, w_{act}. Furthermore the rate between the two displacement measurements are shown w_{act}/w_{opt}.

however the very close agreement between the two different and independent ways of measuring the position shows that both methods give accurate results.

3. Strength measurement of SOFC anode support

To illustrate the methodology and validate it, two experiments are presented here:

I. Two sets of strengths measurements on SOFC anode supports are compared:
   a. One set measured on an Instron machine (Model 1362) at room temperature.
   b. One set measured on the high temperature rig (HT-rig) at room temperature
II. A set of measurements on SOFC anode supports measured at 800 °C in a reducing atmosphere on the high temperature setup.

3.1. Materials

The samples were cut from an anode support of an anode supported SOFC. The anode support is made by tape casting of slurry containing a mixture of nickel-oxide (NiO) powder and yttrium partially stabilized tetragonal zirconia (TZ3Y) powder, which is subsequently sintered. The sintering resulted in an approximately 300 μm thick tape with a porosity of 19%. The porosity was measured by the Archimedes method.

For Experiment I 60 samples of 15 mm by 60 mm were laser cut and tested "as cut". Thus, the flaws from the cuts will influence the strength [17].

For Experiment II another 30 samples of 17 mm by 60 mm were laser cut from the tape and polished down to approximately 15 mm by 60 mm. In order to save time and ensure reproducibility, the samples were stacked and glued together with epoxy, and the stack of samples was then polished by the following procedure: 1) Grinding with: MD Piano 120, MD Piano 220, MD Piano 1200, SiC paper 2400, SiC paper 4000. The samples were washed after every step with water and rinsed with ethanol. 2) Polishing with diamond suspension and blue lubricant polish: MD–DUR with 6 μm diamond suspension, MD–MOL with 3 μm diamond suspension, MD–NAP with 1 μm diamond suspension.

By this procedure a surface finish of approximately 1 μm is achieved and edge defects are effectively removed, as the defects from the laser cutting branches approximately 5–10 μm into a NiO–YSZ support [22]. After polishing the epoxy was removed by heat treatment. The samples were then reduced in-situ as described in the testing procedure. The reduction changes the porosity to 40%.

3.2. Testing procedures

For the high temperature tests, Experiment II, the testing procedure consists of the following two steps:

1. The temperature of the furnace is set to 800 °C and is slowly heated up over 8–9 h, while "safety gas" is continuously supplied to the chamber. The safety gas consists of nitrogen with 9% hydrogen and 91% nitrogen, which will reduce samples completely (see e.g. Ref. [23]).
2. When the temperature of testing is reached, the actuator moves downwards until a change in load of 0.1 N is detected, which indicates contact. Consequently the actuator is moved slightly up, recording of load and displacement is initiated, and the actuator is moved downwards again.

Step 2) is repeated for the 16 samples loaded and the furnace is then brought down to room temperature again. Another 16 samples are loaded and Steps 1) and 2) are repeated. Heating and cooling of the furnace is the time limiting factor. The entire testing procedure for all 32 samples can be completed within two days of work.

The procedure is the same for the room temperature tests, Experiment I, except from that Step 1) was not used.

3.3. Theory

The stress field inside the samples can be obtained by use of Bernoulli–Euler beam theory. From this the variation of the stress, σ_x, along the beam axis (x) and over the vertical axis (z) from an applied load F, can be determined to be a piecewise linear function

$$\sigma_x(x,z) = -\frac{6z}{h^3 w}\begin{cases} F\left(\frac{1}{2}L + x\right) & \text{if} \quad -\frac{1}{2}L \le x < -\frac{1}{4}L \\ \frac{1}{2}FL & \text{if} \quad -\frac{1}{4}L \le x < \frac{1}{4}L \\ F\left(\frac{1}{2}L - x\right) & \text{if} \quad \frac{1}{4}L \le x < \frac{1}{2}L \end{cases} \tag{4}$$

where h is the height of the beam (thickness of sample), w is the width and L is the length of the sample.

For the statistical approach classical Weibull theory is used, where the strength of the samples are ordered by ascending strength and assigned a probability of failure [9]

$$P_{f,i} = \frac{i - 0.5}{N} \quad i = 1, 2, \ldots, N \tag{5}$$

where N is the number of specimens. This set of data is fitted with the least square approach to obtain the characteristic strength, σ_0, and Weibull modulus, m in the Weibull distribution

$$P_f = 1 - \exp\left(-\left(\frac{\sigma_x^{max}}{\sigma_0}\right)^m\right) \tag{6}$$

The effective volume is obtained by integrating the tensional axial stresses over the volume of the sample, V, yielding [7,20]

$$V_{eff} = \int_V \frac{\sigma_x(x,z)}{\sigma_x^{max}} dV = \frac{whL(2+m)}{4(m^2+2m+1)} \tag{7}$$

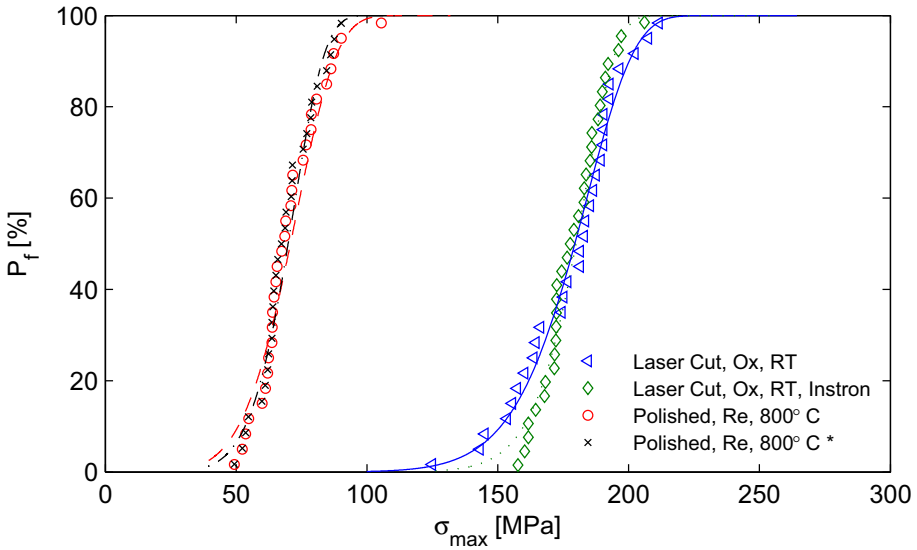

Fig. 8. Weibull plot of the measured strength of SOFC anode supports at room temperature (RT) in oxidized (Ox) conditions, and at 800 °C in reduced (Re) conditions in a reducing atmosphere of ~9% hydrogen and 91% nitrogen. The asterisk shows the Re, 800 °C measurements fitted with the strongest sample omitted.

The beam stiffness, EI, can be extracted from the beam displacement according to Eq. (3). Here the actuator displacement is used, and the elastic modulus, E, can thus be obtained from the slope of the load displacement curve (dF/du) as

$$E = \frac{dF}{du}\frac{3La^2 - 4a^3}{12I} \tag{8}$$

where a is the distance between the loading points and the support points and L is the span between the support points.

4. Results and discussion

4.1. Experiment I

The measured strengths of the anode supports at room temperature are shown in Fig. 8 together with the assigned probabilities of failure and a fit of a Weibull distribution. The results of the Weibull fits are shown in Table 1 together with the mean value and standard deviation of the elastic modulus.

The elastic moduli measured at room temperature in Experiment I.a and I.b are in good agreement. Pihlatie et al. [24] measured the elastic modulus with the impulse excitation technique to 123 GPa for a sample with 19% porosity, which deviates only slightly (~6–12%) from the 131 GPa and 139 GPa measured in this work.

Here 10,000 Monte Carlo simulations have been run. For each simulation 30 samples are probed out of a large pool of samples, which have a known Weibull modulus of 14 (as an example) and a characteristic strength of 185 MPa. Thus, this is similar to the experiment, where 30 samples are chosen randomly and tested. Fig. 9 shows histograms of the outfall of the Monte Carlo

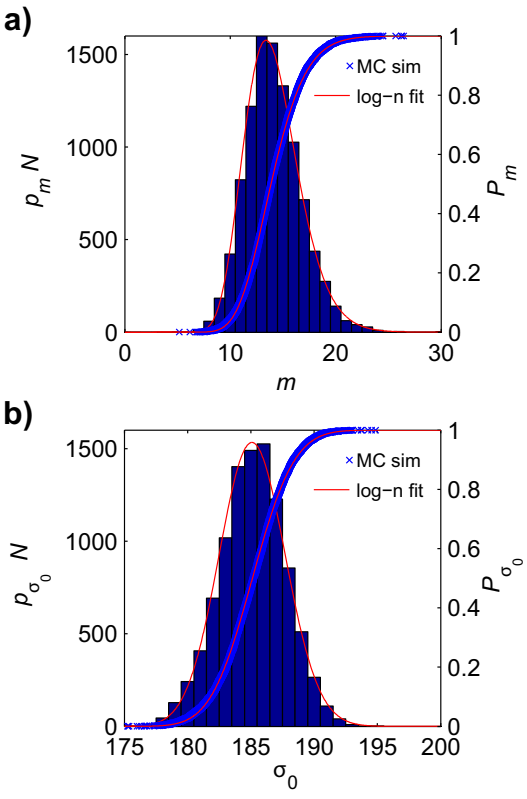

Fig. 9. Histograms, fit of log-normal probability density functions, p, and fit of log-normal cumulative distribution functions, P of Weibull parameters in N = 10,000 Monte Carlo simulations. a) Weibull modulus, m. b) characteristic strength σ_0.

Table 1
Measured characteristic strength, Weibull modulus, effective volume and elastic modulus (±indicates the standard deviation).

Test	Test method	σ_0 [MPa]	m	V_{eff} [mm^3]	E [GPa]
I.a	Instron, RT	186 ± 3.4	11.0 ± 2.1	5.30 ± 1.11	139.1 ± 11
I.b	HT-rig, RT	184 ± 2.3	16.0 ± 3.0	3.67 ± 0.78	131.0 ± 5.4
II	HT-rig, HT	75 ± 2.6	5.7 ± 1.1	10.1 ± 0.77	22.5 ± 4.8

Table 2
Mean value and variance of the log-normal fit to the distribution of the Weibull parameters from the Monte Carlo simulations.

X	Mean (X)	Std (X)	Std (X)/Mean (X)
m	14.1	2.64	0.188
σ_0 [MPa]	185.1	2.62	0.0142

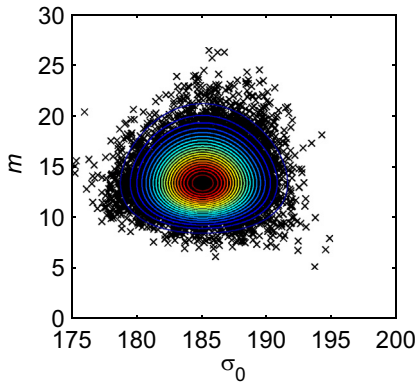

Fig. 10. Characteristic strength σ_0 and Weibull modulus, m, for the 10,000 Monte Carlo simulations. The colors of the contours indicate density levels of the number of simulations going from blue (low) to red (high). (For interpretation of the references to color in this figure legend, the reader is referred to the web version of this article.)

simulations for the a) Weibull modulus and b) characteristic strength. It is clearly seen that the relative variation of the Weibull modulus is significantly higher than of the characteristic strength for the simulations. To quantify this a log-normal distributions have been fitted to the distribution of the two Weibull parameters, see Fig. 9. The mean value and the standard deviation of the log-normal fit are shown in Table 2; the relative standard variation (Std (X)/Mean (X)) of the Weibull modulus can be seen to be a magnitude larger than that of the characteristic strength. In the experiments the deviation between the characteristic strengths is much smaller than the deviation between the Weibull moduli in relation to the standard deviations in the Monte Carlo simulation. A large variation on one parameter can occur while no variation is present for the other, as the two are not correlated. This is demonstrated in Fig. 10 where the Weibull parameters are from the 10,000 simulations are plotted against each other and clearly there are no trends in the data.

In this simulation the probability of $m = 11$ or $m = 16$ is approximately two thirds of the probability of $m = 14$ ($p_{m=11}/p_{m=14} = 0.59$ and $p_{m=16}/p_{m=14} = 0.64$, see Fig. 9). Thus, had the true Weibull modulus of the measured anode support been 14, measurements of the Weibull modulus of 11 or 16 with 30 samples are highly probable outcomes of the experiments simply due to the finite sampling (30 samples only).

As discussed in a publication currently under preparation, an imperfection in the experimental setup will cause larger variations of the measured Weibull parameters. The mean of the Weibull modulus, due to such an imperfection, can also be lowered compared to the true Weibull modulus. In the experiment a larger variation was observed in the high temperature setup, and it cannot be excluded that some inherent imperfection causes this variation. However, in another study a Weibull modulus of 20 has been measured on similar material obtained from a different production batch. This indicates that it is not an inherent imperfection in the equipment that leads to the lower Weibull modulus and the observed deviation between the multi-sample setup and the conventional one sample one is thus ascribed to the limited number of samples.

4.2. Experiment II

The measured strengths of the samples in the reducing atmosphere at 800 °C are shown in Fig. 8 together with the assigned probabilities of failure and a fit of a Weibull distribution. As presented in Table 1 the characteristic strength was determined to be 75 MPa and the Weibull modulus to be 5.6 at an effective volume of 10.2 mm^3. The modulus is relatively low when compared to similar oxidized samples measured at room temperature ($m = 9$–16) [7]. Again the result of the Weibull modulus should be treated with caution. Had the strongest sample not been chosen for testing, a Weibull modulus of 7.5 and a characteristic strength of 74 MPa at an effective volume of 8.3 mm^3 would have been obtained. Thus, a relatively large change of Weibull modulus (∼34%) could be achieved by this slightly different set of samples.

However, it is statistically significant to state that the Weibull modulus has been lowered compared to the measurements in Experiment I. The NiO reduction entails a relatively large volume change, and could initiate flaws, expose inherent flaws in the TZ3Y backbone or generate new internal residual stresses. It is beyond this work the scope of this work to investigate this further.

The characteristic strength of a different type of Ni–YSZ anode support at 800 °C was reported in Ref. [4] to be 67 MPa and the Weibull modulus 13.2 at an effective volume estimated to 9.7 mm^3. In Ref. [4] the Weibull modulus was obtained from an average over all tested samples. Except from the low Weibull modulus obtained in this work these values are comparable. Further investigations on the strength of SOFC anode supports at high temperatures are currently being carried out to elucidate independently effects of temperature, porosity, reduction temperature and the state of the Ni (Ni or NiO).

The elastic modulus at 800 °C of a reduced sample (Ni–YSZ) with a porosity of 38% was measured by impulse excitation technique to 55.8 GPa in Ref. [24]. The elastic modulus is here measured to 22.5 ± 4.8 GPa, which is significantly lower (∼60% smaller). In the experiments in this work the samples are reduced from room temperature, which is known to result in a microstructure different from the one obtained if reducing gasses are introduced after the samples have been brought to high temperature [25]. Differences in microstructure due to the different reduction procedure is assumed to be the main reason for the strongly reduced E-modulus observed here compared to Ref. [24].

5. Conclusions

This work presents a novel, efficient and accurate strength measurement method to test the ceramics in electrochemical conversion devices such as SOFCs and SOECs at operating conditions (high temperature and either oxidizing or reducing atmosphere).

A number of technical developments lead to this achievement, but the main novelty was the use of a special fixture for four point bending, which both serves as a sample holder for up to 16 specimens and as a loading device.

The accuracy achieved is both related to the feasible high number of samples that can be tested and due to a design where effects of friction from sealings or bellows on the load measurements are avoided. Friction was also avoided on the displacement measurements by a camera and by novel optical detection methods, where prior knowledge of the shape of the bending sample was used to achieve higher accuracy. Comparing the optical displacement detection with the movement of the actuator demonstrates a high accuracy showing only 0.7% deviation between the two methods.

The measurement technique was applied in two experiments on solid oxide fuel cell anode supports of porous Ni–3SYZ. The first experiment compared the measurements from a single sample Instron machine at room temperature with the high temperature multi-sample setup running at room temperature. This experiment showed identical characteristic strength and elastic moduli, but some variation of the Weibull modulus. The variation could be explained by the randomness of sample selection and the finite number of samples.

The second experiment demonstrated the measurement of the strength of a set of specimens of anode supports of solid oxide fuel cell under reducing conditions (9% hydrogen and 91% nitrogen) at 800 °C. The characteristic strength was found to be 75 MPa and the Weibull modulus to 5.7 at an effective volume of 10.2 mm^3. It was shown that only small variation in the experiment may change the Weibull modulus significantly (~34%). The elastic moduli measured at higher temperatures were relatively small (~60% smaller) compared to previously measured elastic moduli. The deviation was speculated to be due to microstructural differences following from different reduction routes.

Acknowledgments

The authors would like to acknowledge Topsøe Fuel Cell A/S for financial support, Bjørn Sejr Johansen for several technical ideas and solutions on the rig design, John Johnson, Kristian Nim Sørensen, and Jens Østergaard, for their assistance with manufacturing and design, and Ebtisam Abdellahi for assistance with sample preparation.

References

[1] L. Grahl-Madsen, P.H. Larsen, N. Bonanos, J. Engell, S. Linderoth, J. Mater. Sci. 41 (2006) 1097–1107.
[2] M. Radovic, E. Lara-Curzio, Acta Mater. 52 (2004) 5747–5756.
[3] J. Malzbender, R.W. Steinbrech, J. Eur. Ceram. Soc. 28 (2008) 247–252.
[4] J. Malzbender, R.W. Steinbrech, L. Singheiser, Adv. Solid Oxide Fuel Cells 26 (2005) 293–298.
[5] E. Lara-Curzio, M. Radovic, R.M. Trejo, C. Cofer, T.R. Watkins, K.L. More, Effect of Thermal Cycling and Thermal Aging on the Mechanical Properties of, and Residual Stresses in, Ni-Ysz/ysz Bi-layers, in: Advances in Solid Oxide Fuel Cells II, vol. 27, 2007, pp. 383–391. http://onlinelibrary.wiley.com/doi/10.1002/9780470291337.ch37/summary.
[6] A. Faes, H.L. Frandsen, M. Pihlatie, A. Kaiser, D.R. Goldstein, J. Fuel Cell Sci. Technol. 7 (2010) 051011.
[7] H.L. Frandsen, T. Ramos, A. Faes, M. Pihlatie, K. Brodersen, J. Eur. Ceram. Soc. 32 (2012) 1041–1052.
[8] A. Nakajo, J. Kuebler, A. Faes, et al., Ceram. Int. 38 (2012) 3907–3927.
[9] A. Khalili, K. Kromp, J. Mater. Sci. 26 (1991) 6741–6752.
[10] A. Atkinson, A. Selcuk, in: Proceedings of the Fifth International Symposium on Solid Oxide Fuel Cells (Sofc-V), vol. 97, 1997, pp. 671–680.
[11] A. Atkinson, A. Selcuk, Acta Mater. 47 (1999) 867–874.
[12] A. Atkinson, A. Selcuk, Solid State Ionics 134 (2000) 59–66.
[13] F.L. Lowrie, R.D. Rawlings, J. Eur. Ceram. Soc. 20 (2000) 751–760.
[14] A. Selcuk, A. Atkinson, J. Am. Ceram. Soc. 83 (2000) 2029–2035.
[15] J.H. Andreasen, J. Am. Ceram. Soc. 76 (1993) 2933–2935.
[16] S.B. Batdorf, H.L. Heinisch, J. Am. Ceram. Soc. 61 (1978) 355–358.
[17] T. Klemenso, E. Lund, B.F. Sorensen, J. Am. Ceram. Soc. 90 (2007) 1827–1835.
[18] W. Weibull, The phenomenon of rupture in solids, Generalstabena Litografiska Anstalts Forlag, Stockholm, 1939, p. 55.
[19] H.L. Frandsen, Mech. Mater. (2014) in press.
[20] R. Danzer, J. Eur, Ceram. Soc. 10 (1992) 461–472.
[21] L. Blum, H. Buchkremer, S. Gross, A. Gubner, L.G.J. de Haart, H. Nabielek, W.J. Quadakkers, U. Reisgen, M.J. Smith, R. Steinberger-Wilckens, R.W. Steinbrech, F. Tietz, I.C. Vinke, Fuel Cells 7 (2007) 204–210.
[22] S. Goutianos, H.L. Frandsen, B.F. Sorensen, J. Eur, Ceram. Soc. 30 (2010) 3173–3179.
[23] T. Klemenso, M. Mogensen, J. Am, Ceram. Soc. 90 (2007) 3582–3588.
[24] M. Pihlatie, A. Kaiser, M. Mogensen, J. Eur. Ceram. Soc. 29 (2009) 1657–1664.
[25] Y. Wang, M.E. Walter, K. Sabolsky, M.M. Seabaugh, Solid State Ionics 177 (2006) 1517–1527.